Theoretical and Experimental Analysis of 1.3-μm InGaAsN/GaAs Lasers

Stanko Tomić, Eoin P. O'Reilly, *Member, IEEE*, Robin Fehse, Stephen John Sweeney, *Member, IEEE*, Alfred R. Adams, *Fellow, IEEE*, Aleksey D. Andreev, Stelios A. Choulis, Thomas J. C. Hosea, and Henning Riechert

***Abstract*—We present a comprehensive theoretical and experimental analysis of 1.3-μm InGaAsN/GaAs lasers. After introducing the 10-band $\mathbf{k}\cdot\mathbf{p}$ Hamiltonian which predicts transition energies observed experimentally, we employ it to investigate laser properties of ideal and real InGaAsN/GaAs laser devices. Our calculations show that the addition of N reduces the peak gain and differential gain at fixed carrier density, although the gain saturation value and the peak gain as a function of radiative current density are largely unchanged due to the incorporation of N. The gain characteristics are optimized by including the minimum amount of nitrogen necessary to prevent strain relaxation at the given well thickness. The measured spontaneous emission and gain characteristics of real devices are well described by the theoretical model. Our analysis shows that the threshold current is dominated by nonradiative, defect-related recombination. Elimination of these losses would enable laser characteristics comparable with the best InGaAsP/InP-based lasers with the added advantages provided by the GaAs system that are important for vertical integration.**

***Index Terms*—1.3-μm laser emission, dilute nitride materials, InGaAsN, optical fiber telecommunications, semiconductor devices modeling, semiconductor lasers.**

I. INTRODUCTION

SINCE dilute nitride III-V compounds have been proposed by Kondow [1] for the realization of semiconductor quantum well (QW) laser diodes emitting at the 1.3-μm optical window, there has been considerable research effort in both material and optoelectronic device physics of this novel material. It has been found that replacing a small amount of the group V element by nitrogen in a III–V compound reduces the energy gap. This reduction (of about 0.1 eV per % of N for $x < \sim 0.03$) occurs because of a band anticrossing (BAC) interaction between the conduction band edge and a higher-lying nitrogen resonant band [2] and dramatically changes the electronic structure [3], thus offering a new route to band structure engineering and improved optoelectronic properties. In particular, the growth of strained InGaAsN/GaAs QW structures allows the benefits of compressive strain and of growth on a GaAs substrate. In addition, the inclusion of N in the InGaAsN layers increases the conduction band offset, leading to improved electron confinement and to decreased electron spill out at room temperature and above, when compared with conventional InGaAsP 1.3-μm lasers. Although edge-emitting and VCSEL laser structures with impressive characteristics have already been reported [4]–[6] the influence of N on the electronic structure and laser characteristics has not yet been fully elucidated.

In this paper, we aim to present a comprehensive theoretical and experimental analysis of the electronic structure of dilute nitride alloys, and the consequences of that electronic structure for 1.3-μm laser emission. We begin in the next section by introducing the ten-band $\mathbf{k}\cdot\mathbf{p}$ Hamiltonian used to calculate the band structure of InGaAsN heterostructures. After describing the gain model that we use, we discuss the effect of nitrogen on band alignments in strained heterostructures, refining the band structure parameters by comparison with photoreflectance measurements. This analysis provides us with a suitable framework in which to calculate the gain and spontaneous emission characteristics of ideal InGaAsN laser structures. We analyze the influence of nitrogen incorporation on the calculated dipole matrix elements, electron effective mass, strain, gain versus carrier concentration and radiative current characteristic, as well as its influence on differential gain. We then apply the model to analyze the measured characteristics of two sets of 1.3-μm InGaAsN lasers, one set with a single quantum well (SQW) and the other with a triple quantum well (TQW) active region. By comparing the calculated and measured spontaneous emission spectra we found that a secant-hyperbolic line broadening function gave a good description of the experimental spectra, and extracted the temperature dependent broadening energy which provides the best fit between the measured and calculated radiative currents at threshold. We then used this information to deduce the carrier concentration at threshold, n_{th}, for both devices and its dependence on temperature. We use the calculated value of n_{th} in conjunction with experimental measurements to analyze the relative contributions to the threshold current of radiative recombination and of nonradiative monomolecular and Auger-related recombination processes. We show that the monomolecular, radiative and Auger coefficients are the same for both lasers, and that the threshold current at room temperature is dominated by monomolecular, defect-related recombination. Finally, we briefly compare the theoretically estimated laser characteristics of InGaAsN-based and conventional InGaAsP-based 1.3-μm lasers.

Manuscript received February 26, 2003; revised July 30, 2003. This work was supported in part by Engineering and Physical Sciences Research Council (EPSRC) U.K., Science Foundation Ireland, and Infineon Technologies.

S. Tomić was with Department of Physics, University of Surrey, Guildford, Surrey GU2 7XH, U.K. He is now with Department of Physics and Astronomy, University of Sheffield, Sheffield S3 7RH, U.K. (e-mail: s.tomic@dl.ac.uk; s.tomic@sheffield.ac.uk).

E. P. O'Reilly is with NMRC, University College, Lee Maltings, Cork, Ireland (e-mail: eoin.oreilly@nmrc.ie).

R. Fehse, S. J. Sweeney, A. R. Adams, A. D. Andreev, and T. J. C. Hosea are with Department of Physics, University of Surrey, Guildford, Surrey GU2 7XH, U.K. (e-mail: alf.adams@surrey.ac.uk).

S. A. Choulis is with The Blackett Laboratory, Imperial College of Science Technology and Medicine, London SW7 2BZ, U.K.

H. Riechert is with Infineon Technologies AG, Munich D-81730, Germany.

Digital Object Identifier 10.1109/JSTQE.2003.819516

1077-260X/03$17.00 © 2003 IEEE

Authorized licensed use limited to: University of Surrey. Downloaded on May 26, 2009 at 10:31 from IEEE Xplore. Restrictions apply.

II. THEORETICAL METHOD

A. 10 Band $\mathbf{k}\cdot\mathbf{p}$ Hamiltonian

The $\mathbf{k}\cdot\mathbf{p}$ and envelope function methods are widely applied to study III-V semiconductor heterostructures [7]. In this section, we extend the well-established 8 band $\mathbf{k}\cdot\mathbf{p}$ Hamiltonian [8] by introducing two additional spin degenerate nitrogen-related states. The strong interaction between the N resonant states and the conduction band edge means that the conventional 8-band $\mathbf{k}\cdot\mathbf{p}$ method cannot be applied to InGaAsN and related heterostructures. We must include the interaction between the N resonant states and the conduction band edge to describe the variation of the (zone-center) conduction band edge energy with N. This leads to a modified ten-band $\mathbf{k}\cdot\mathbf{p}$ Hamiltonian for InGaAsN as shown in (1) at the bottom of the page, where we only show the upper triangular block because the matrix is Hermitian. The matrix elements

$$\begin{aligned}
E_{\rm CB} &= E_{c0} + \frac{\hbar^2}{2m_0} s_c\left(k_{\|}^2 + k_z^2\right) + \delta E_{\rm CB}^{hy}\\
E_{\rm HH} &= E_{v0} - \frac{\hbar^2}{2m_0}(\gamma_1+\gamma_2)k_{\|}^2 - \frac{\hbar^2}{2m_0}(\gamma_1 - 2\gamma_2)k_z^2\\
&\quad + \delta E_{\rm VB}^{hy} - \eta_{ax}\\
E_{\rm LH} &= E_{v0} - \frac{\hbar^2}{2m_0}(\gamma_1-\gamma_2)k_{\|}^2 - \frac{\hbar^2}{2m_0}(\gamma_1 + 2\gamma_2)k_z^2\\
&\quad + \delta E_{\rm VB}^{hy} + \eta_{ax}\\
E_{\rm SO} &= E_{v0} - \Delta_{so} - \frac{\hbar^2}{2m_0}\gamma_1\left(k_{\|}^2 + k_z^2\right) + \delta E_{\rm VB}^{hy}\\
T_{\pm} &= \frac{1}{\sqrt{6}}P(k_x \pm i k_y)\\
U &= \frac{1}{\sqrt{3}}P k_z\\
S &= \sqrt{\frac{3}{2}}\frac{\hbar^2}{m_0}\gamma_3 k_z (k_x - i k_y)\\
R &= \frac{\sqrt{3}}{2}\frac{\hbar^2}{2m_0}[(\gamma_2+\gamma_3)(k_x - ik_y)^2\\
&\quad - (\gamma_3 - \gamma_2)(k_x + ik_y)^2]\\
Q &= -\frac{1}{\sqrt{2}}\frac{\hbar^2}{m_0}\gamma_2 k_{\|}^2 + \sqrt{2}\frac{\hbar^2}{m_0}\gamma_2 k_z^2 - \sqrt{2}\eta_{ax}
\end{aligned} \tag{2}$$

are the same as in the conventional 8-band Hamiltonian, where $k_{\|}^2 = k_x^2 + k_y^2$, and the subscripts CB, HH, LH, and SO stand for conduction, heavy-hole, light-hole, and split-off bands, respectively. The nitrogen resonant band is labeled by N, with

$$E_{\rm N} = E_{N0} + \delta E_{\rm N}^{hy} \tag{3}$$

while

$$V_{Nc} = \beta\sqrt{x} \tag{4}$$

describes the coupling between the N states and the conduction band edge, including its dependence on nitrogen composition, x. The parameter $s_c = 1/m_c^* - (E_P/3)[2/E_g^h + 1/(E_g^h + \Delta_{so})], \gamma_1 = \gamma_1^L - E_P/(3E_g^h), \gamma_{2,3} = \gamma_{2,3}^L - E_P/(6E_g^h)$ are modified Luttinger–Kohn parameters, Δ_{so} the magnitude of the spin-orbit splitting at $k_{\|} = 0$, and $P = -i(\hbar/m_0)\langle s'|p_v|v\rangle$ is the Kane matrix element for the conduction band ($E_P = 2m_0P^2/\hbar^2$) where $|s'\rangle$ indicates a CB Bloch state of s-like symmetry and $|v\rangle$ is a valence band p state, with character ($|v\rangle = |x\rangle, |y\rangle$ or $|z\rangle$), and E_g^h is the host material (unperturbed) energy gap. $\delta E_b^{hy} = -2a_b(1 - c_{12}/c_{11})\varepsilon_{xx}$ and $\eta_{ax} = -b_{ax}(1 + 2c_{12}/c_{11})\varepsilon_{xx}$ describe the influence of the hydrostatic and shear strain components on the band structure, where a_b are hydrostatic deformation potentials (with index b =N, CB, and VB for nitrogen, conduction and valence band respectively); c_{11} and c_{12} are elastic constants, b_{ax} the axial deformation potential and ε_{xx} is the strain in the layer plane. There are far more N-related parameters in the Hamiltonian of (1) than can be accurately determined experimentally. Symmetry arguments indicate that the matrix elements $T_{N\pm}$ and U_N should vary linearly with k, coupling the N level to the valence band. The sp^3s^* tight-binding (TB) calculations provide a guide as to which are the most important parameters [9], [10]. We find that the dominant terms are those which are independent of $\mathbf{k}$, and included in (1) to describe the variation of the overall energy gap with N composition. Consequently, we set $T_{N\pm}$ and U_N to be zero.

$$\begin{pmatrix}
E_{\rm N} & V_{Nc} & -\sqrt{3}T_{N+} & \sqrt{2}U_N & -U_N & 0 & 0 & 0 & -T_{N-} & -\sqrt{2}T_{N-}\\
 & E_{\rm CB} & -\sqrt{3}T_{+} & \sqrt{2}U & -U & 0 & 0 & 0 & -T_{-} & -\sqrt{2}T_{-}\\
 & & E_{\rm HH} & \sqrt{2}S & -S & 0 & 0 & 0 & -R & -\sqrt{2}R\\
 & & & E_{\rm LH} & Q & T_{N+}^* & T_{+}^* & R & 0 & \sqrt{3}S\\
 & & & & E_{\rm SO} & \sqrt{2}T_{N+}^* & \sqrt{2}T_{+}^* & \sqrt{2}R & -\sqrt{3}S & 0\\
 & & & & & E_{\rm N} & V_{Nc} & -\sqrt{3}T_{N-} & \sqrt{2}U_N & -U_N\\
 & & & & & & E_{\rm CB} & -\sqrt{3}T_{-} & \sqrt{2}U & -U\\
 & & & & & & & E_{\rm HH} & \sqrt{2}S^* & -S^*\\
 & & & & & & & & E_{\rm LH} & Q\\
 & & & & & & & & & E_{\rm SO}
\end{pmatrix}
\begin{matrix}
|u_1\rangle\\ |u_2\rangle\\ |u_3\rangle\\ |u_4\rangle\\ |u_5\rangle\\ |u_6\rangle\\ |u_7\rangle\\ |u_8\rangle\\ |u_9\rangle\\ |u_{10}\rangle
\end{matrix} \tag{1}$$

Authorized licensed use limited to: University of Surrey. Downloaded on May 26, 2009 at 10:31 from IEEE Xplore. Restrictions apply.

B. Gain Model

The laser gain is calculated using a model based on density matrix theory [11], [12]. The gain and spontaneous emission spectra are given by

$$G(\hbar\omega) \propto \left(\frac{1}{\hbar\omega}\right) \int_{k_\parallel} |M_{e-h}|^2 \rho^{2D}(k_\parallel)\{f[E_e(k_\parallel)] - f[E_h(k_\parallel)]\}\mathcal{S}(\hbar\omega)dk_\parallel \tag{5}$$

$$R_{sp}(\hbar\omega) \propto (\hbar\omega) \int_{k_\parallel} |M_{e-h}|^2 \rho^{2D}(k_\parallel) f[E_e(k_\parallel)] \times \{1 - f[E_h(k_\parallel)]\}\mathcal{S}(\hbar\omega)dk_\parallel \tag{6}$$

respectively, where $|M_{e-h}|^2$ is the k- and subband-dependent optical dipole matrix element for allowed electron-hole transitions, $\rho^{2D} = k_\parallel/(2\pi L_z)$ is the quantum well (2D) density of states, and $f[E_{e(h)}]$ the Fermi function for electrons (holes). We used a secant-hyperbolic function to model the line broadening of the spontaneous emission and gain spectra [13]

$$\mathcal{S}(\hbar\omega) = \frac{1}{\pi\delta}\mathrm{sech}\left(\frac{E_e(k_\parallel) - E_h(k_\parallel) - \hbar\omega}{\delta}\right) \tag{7}$$

where $\delta = \hbar/\tau_{in}$ is the line broadening. The calculated spontaneous emission spectra at threshold were fitted to measured spectra between 30–300 K. We found better agreement between experiment and theory using the sech function rather than the Lorenzian function commonly used to model line broadening in semiconductor lasers. The threshold gain g_{th} was determined by substituting appropriate experimental and calculated values (as described later) into the formula

$$g_{\mathrm{th}} = \frac{1}{\Gamma}\left(\alpha_i + \frac{1}{L}\ln\frac{1}{R}\right) \tag{8}$$

where Γ is the optical confined factor, α_i the internal losses, L the cavity length and R the reflectivity of the mirrors.

III. Results and Discussion

We review here how we derive the band structure parameters, Section III-A, before presenting calculations of QW band structure in Section III-B. We present gain calculations in the following Section III-C, where we derive general conclusions about the gain characteristics of InGaAsN 1.3-μm lasers. The results of the gain calculations are then used to inform the analysis of real devices in Section III-D.

A. Band Lineups

The values of the conduction and valence band offsets have a significant influence on the carrier confinement and the gain characteristics of semiconductor quantum well laser structures. As an example, carrier spillover into the conduction band decreases the differential gain in InGaAsP/InP 1.3- and 1.5-μm lasers [14]. There is still debate concerning the band offset ratios in InGaAsN/GaAs QW structures. Although a type II band alignment was originally proposed for $GaAs_{1-x}N_x$ heterojunctions, based on band offsets calculated using the dielectric model [15], more recent first-principles calculations [16] as well as three independent experimental techniques: time-resolved photoluminescence (PL) spectroscopy, PL polarization, and optically detected cyclotron resonance [17], strongly supported a type I alignment.

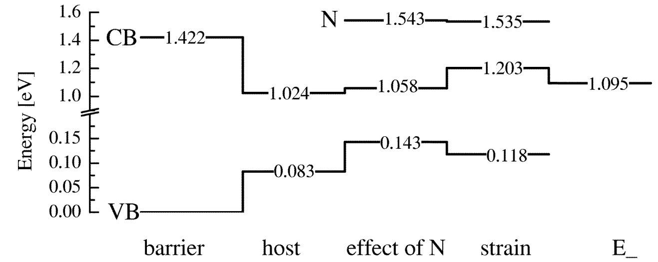

Fig. 1. Band edge lineup for $In_{0.36}Ga_{0.64}As_{0.983}N_{0.017}$ pseudomorphically lattice matched on GaAs.

We have fitted the input parameters for our band structure calculations to photoreflectance (PR) spectra from a range of InGaAsN/GaAs quantum well (QW) samples. The parameters derived for the quaternary alloys are consistent with more extensive measurements on GaAsN/GaAs heterostructures [18]. For band structure calculations, we assume that the energy of the nitrogen level E_{N0}, conduction E_{c0}, and valence E_{v0} band edge energies at the Γ_6 point all vary linearly with N composition x relative to the valence band maximum of the GaAs barrier ($E_{v0}^b = 0$). We assume for $InGaAs_{1-x}N_x$ that

$$E_{c0}^w = \left(E_{v0}^b + E_v^{\mathrm{offset}} + E_g^h\right) - \alpha x + \kappa x \tag{9}$$

$$E_{v0}^w = E_{v0}^b + E_v^{\mathrm{offset}} + \kappa x \tag{10}$$

while the N resonant state energy, E_N was set at

$$E_{N0} = E_{c0}^w + \Delta E_{Nc} - \gamma x + \kappa x \tag{11}$$

where the superscript $w(b)$ refers to the well (barrier) layers, respectively, ΔE_{Nc} is the energy separation between the nitrogen resonant level and the bottom of the host material conduction band, and α and γ determine the variation of the $InGaAs_{1-x}N_x$ energy gap with composition, x, while κ gives the chemical valence band offset, describing how the valence band edge of unstrained $InGaAs_{1-x}N_x$ shifts on an absolute energy scale with respect to that of a GaAs barrier [18]. For $In_yGa_{1-y}As_{1-x}N_x$, we first use model solid theory [19] to determine the relative band alignment and the valence band offset E_v^{offset} of the $In_yGa_{1-y}As$ well material relative to GaAs, and then use (9)–(11) to introduce the band offset variation with N composition, x. Fig. 1 shows how band line ups are calculated in the $In_{0.36}Ga_{0.64}As_{0.983}N_{0.017}$/GaAs SQW structure, whose gain and laser characteristics we investigate later. In the section "barrier/host," the bands are lined up relative to the average valence band level, ignoring any strain effects. The section labeled "effect of N" shows how the inclusion of nitrogen modifies the unstrained band line up, i.e., the effect of the parameters α, γ and κ, while "strain" indicates how the CB and HH band edges shift when strain effects are included, using interpolated alloy deformation potentials to describe the effects of the built-in hydrostatic and axial strain in the QW

Authorized licensed use limited to: University of Surrey. Downloaded on May 26, 2009 at 10:31 from IEEE Xplore. Restrictions apply.

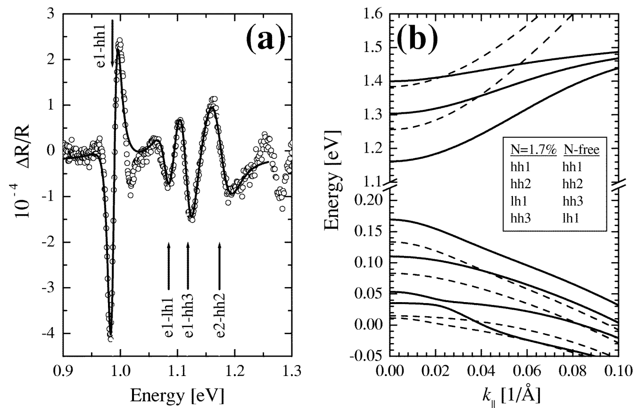

Fig. 2. (a) Experimental 300 K photomodulated reflectance spectrum of the $In_{0.36}Ga_{0.64}As_{0.983}N_{0.017}$/GaAs SQW 1.3-$\mu$m laser device structure of Section III.D (circles). The full curve shows a least-squares fit with an appropriate four-oscillator line shape model, using constrained energies obtained from the $\mathbf{k}\cdot\mathbf{p}$ theory (vertical arrows). (b) Solid line-calculated band structure of $In_{0.36}Ga_{0.64}As_{0.983}N_{0.017}$/GaAs SQW laser device based on the experimentally observed QW transitions at $k_{\|} = 0$ depicted in (a). The excitonic binding energies red-shifted QW transitions by $-6.8, -7.1, -6.3$, and -7.4 meV for the $e1hh1; e1lh1; e1hh3$ and $e2hh2$, respectively. The corresponding final red-shifts due to the quantum confinement Stark effect were ≤ -0.5 meV for $e1hh1$ and $e2hh2$ (and so are negligible) and -1.0 meV for $e1lh1$: The largest QCSE shift was -10 meV for $e1hh3$ due to the close proximity of the $hh3$ state to the barrier edge. The resulting final set of predicted QW energies were 0.985, 1.102, 1.119, and 1.187 eV [21]. Dashed line-band structure of an equivalent N-free: $In_{0.36}Ga_{0.64}As$/GaAs QW. Legend: order of VB subband characters from the bottom to the top of the VB quantum well.

[(2) and (3)]. Finally, E_{-} indicates how the CB edge is shifted downwards due to its interaction with the N resonant states.

We assume $\gamma = \kappa$, consistent with our previous analysis of GaAsN/GaAs structures [18], and also choose the same value of κ as in GaAsN to describe the variation of the VB band offset with nitrogen content in InGaAsN. Previously, we have analyzed three wide $GaAs_{1-x}N_x$/GaAs QW samples, with well width $L_{\rm QW} \sim 25$ nm [18], where we observed a large number of transitions in each sample, despite the built-in tensile strain, and consistent with heavy-hole confinement in the VB due to the incorporation of nitrogen [18]. By changing the value of the valence band offset parameter κ in our model, and comparing the number and energy of the experimentally observed transitions with allowed en-hh$n$ and en-lh$n$ transitions calculated by our ten-band $\mathbf{k}\cdot\mathbf{p}$ model we conclude that the value of κ should be at least 3.5 eV. This agrees with an earlier estimate of 30% ± 5% for the valence band offset obtained by tracking the e1-lh1 and e1-hh1 crossover in narrow GaAsN QWs [20].

B. Quantum Well Band Structure

Fig. 2(a) shows experimental room temperature photo-modulated reflectance (PR) measurements of a piece of as-grown wafer of a dilute-N InGaAsN SQW structure [21]. One of the laser devices studied in this paper was fabricated from the same wafer (see Section III-D). By matching the measured and calculated QW transition energies in this, and a range of similar dilute-N InGaAsN structures as a function of pressure [22], we have deduced the N-related input parameters for our band structure calculations. We set $\alpha = 1.55$ eV, $\gamma = \kappa = 3.5$ eV. V_{Nc} was calculated using the tight-binding method, which includes the effect of different nitrogen nearest neighbor environments, and was found to vary with N composition, x, as $V_{Nc} = 1.675\sqrt{x}$ eV [23]. This dependence is consistent with other recent experimental work for high indium content samples, [24] but significantly weaker than that reported previously for samples with lower In content between 0 and 0.08 (where V_{Nc} varied from $2.3\sqrt{x}$ to $2.7\sqrt{x}$ eV) [25], [26]. We assumed the energy separation between the N level and the bottom of the host material CB to be independent of indium composition in unstrained InGaAsN, $\Delta E_{Nc} = 0.485$ eV [10], [23].

Matching theory with the experimental results at $k_{\|} = 0$ in Fig. 2(a) we have used the full ten-band $\mathbf{k}\cdot\mathbf{p}$ model to predict the band structure and dispersion of the confined energy levels in the SQW laser, as shown in Fig. 2(b). A strong nonparabolicity is clearly visible in the CB dispersion, due to its interaction with the N-resonant level, which also results in a strong deepening of the CB well. The well CB edge would be at 1.203 eV if $V_{Nc} = 0$ (all energies are given relative to the VB edge in the GaAs barrier material), but the strong N-CB interaction pushes it down significantly, to a value of $E_{-} = 1.095$ eV, Fig. 1, leading to a conduction band offset of $\Delta E_c^{\rm offset} = 327$ meV. At room temperature, the energies of the first QW confined CB state, and the quasi-Fermi level E_{Fc} at the threshold carrier concentration ($n_{\rm th} = 2.26 \times 10^{12}$ cm^{-2}), are calculated to be 62 and 122 meV above E_{-}, respectively. The energy difference between E_{Fc} and the GaAs barrier CB edge is ~200 meV. This large offset should ensure negligible probability of electron occupation in the barriers at room temperature. Thus, in spite of the large volume of the GaAs barrier, and separate confinement heterostructure (SCH) layers, the carrier density in these layers is negligible. Also, the inclusion of 1.7% of N reduces the QW compressive strain (with respect to InGaAs with In = 36%) from $\varepsilon_{xx} = 2.51\%$ to $\varepsilon_{xx} = 2.19\%$.

C. Gain Characteristics of Ideal InGaAsN QW Laser

We reviewed that the band structure of InGaAsN/GaAs heterostructures differs significantly from that of conventional III-V heterostructures, due to the band anti-crossing interaction between the N resonant states and the conduction band edge. We turn here to investigate the consequences of that coupling for optical gain and lasing in ideal InGaAsN/GaAs QW lasers. We compare first the gain characteristics of an ideal InGaAsN 1.3-μm laser with an equivalent N-free structure, showing that the incorporation of N modifies the variation of gain with carrier density, but not with radiative current density. We then consider specific InGaAsN-based QW structures, from which we conclude that optimum performance is likely to be obtained by minimizing the N content in a 1.3-μm InGaAsN/GaAs QW laser. These calculations will then inform our discussion of real devices in the next section.

The coupling between the N level and the conduction band edge modifies the conduction band wavefunctions and reduces the interband optical transition matrix element $|M_{e-h}|^2$ compared to a N-free conventional III-V alloy. Fig. 3 shows the calculated variation as a function of in-plane wavevector $k_{\|}$ for the TE and TM interband matrix elements linking the first confined electron (e1) with heavy-hole (hh1) and light-hole (lh1) states for an ideal 7-nm-wide $In_{0.36}Ga_{0.64}As_{0.98}N_{0.02}$/GaAs

Authorized licensed use limited to: University of Surrey. Downloaded on May 26, 2009 at 10:31 from IEEE Xplore. Restrictions apply.

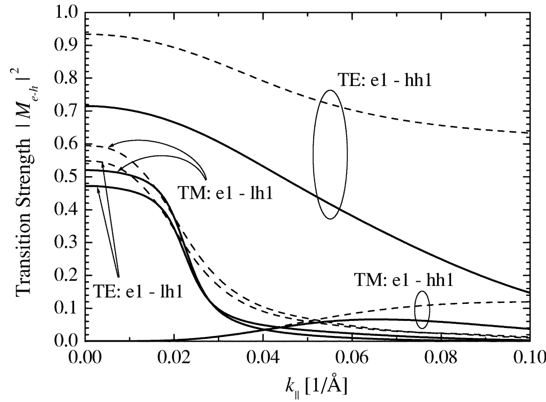

Fig. 3. Dipole matrix elements for TE and TM polarized transitions between the first conduction subband (e1) and first heavy-hole (hh1) and light-hole (lh1) subbands in a 6.4 nm $In_{0.36}Ga_{0.64}As_{0.983}N_{0.017}$/GaAs (solid lines) and $In_{0.36}Ga_{0.64}$As/GaAs QW structure (dashed lines) at $T = 300$ K.

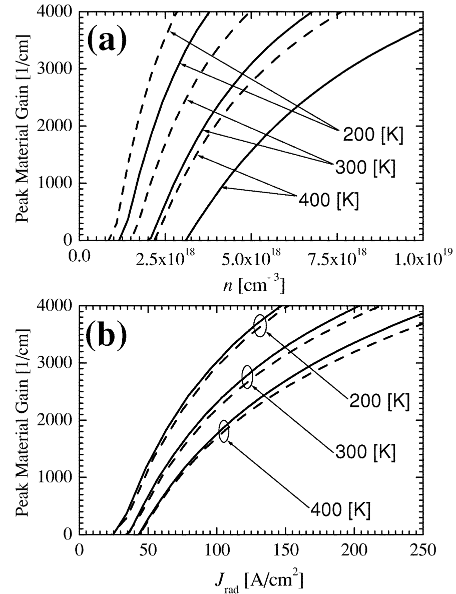

Fig. 4. Temperature dependence of the peak material TE gain: (a) as a function of carrier density and (b) as a function of radiative current density. Solid line—7-nm $In_{0.36}Ga_{0.64}As_{0.98}N_{0.02}$/GaAs SQW laser and dashed lines are the same dependence for an equivalent nitrogen-free structure.

QW laser structure. The band edge, zone-center, TE matrix element is calculated to decrease by ~30% due to the incorporation of N. The nitrogen-conduction band coupling, therefore, leads to an increased conduction band edge effective mass. We calculate that the band edge density-of-states effective mass in the first conduction subband increases to $0.066m_0$ for $\mathrm{N} = 2\%$, which represents ~30% increase over that of the host material ($0.051m_0$ for $\mathrm{In} = 36\%$ and N-free QW).

The reduction in $|M_{e-h}|^2$ and consequent increase in the conduction band edge effective mass, m_c^* causes the product $m_c^* \times |M_{e-h}|^2$ to stay approximately constant, as would be expected from $\mathbf{k} \cdot \mathbf{p}$ theory: the dominant contribution to the inverse effective mass, m_c^{*-1}, is directly proportional to $|M_{e-h}|^2$. The band structure and matrix elements presented in Fig. 3 were used to calculate the variation of material gain with temperature T and as a function of carrier density n and of radiative current density J_{rad} both in a $In_{0.36}Ga_{0.64}As_{0.98}N_{0.02}$/GaAs QW structure, and in an equivalent N-free structure [27]. The gain and spontaneous emission spectra were calculated using (5) and (6) with the intraband relaxation time τ_{in} assumed to have a constant value in the ideal case of $\tau_{in} = 0.1$ ps. We first determined the electron and hole quasi-Fermi energies, E_{Fc} and E_{Fv} as a function of n and T. The increase in the conduction band effective mass leads to an increase in the carrier concentration at transparency for the $In_{0.36}Ga_{0.64}As_{0.98}N_{0.02}$/GaAs QW laser structure and a decrease in the quasi-Fermi energy separation $E_{Fc} - E_{Fv}$ for a fixed carrier concentration. As a consequence the peak gain decreases at a fixed carrier density in the $In_{0.36}Ga_{0.64}As_{0.98}N_{0.02}$ structure when compared to an equivalent, N-free $In_{0.36}Ga_{0.64}$As/GaAs QW structure, Fig. 4(a). There is however a much weaker variation in the peak gain versus radiative current density, Fig. 4(b). This weak variation reflects the fact that for a fixed quasi-Fermi level separation, the radiative current J_{rad} in a QW laser is approximately proportional to $m_r^* \times |M_{e-h}|^2$, where m_r^* is the band edge reduced effective mass. Because the VB mass, m_v^*, is always larger than the CB mass m_c^*, the reduced mass m_r^* is determined primarily by m_c^*. From $\mathbf{k} \cdot \mathbf{p}$ theory, $1/m_c^* \propto |M_{e-h}|^2$, so that $m_r^* \times |M_{e-h}|^2 \approx$ constant, thus accounting for the calculated weak variation in J_{rad}, as noted previously by Chow *et al.* [28] using an eight-band $\mathbf{k} \cdot \mathbf{p}$ model, but a phenomenological formula for the energy gap and electron effective mass. Likewise, because of the reduced interband matrix element, there is little difference in the calculated gain as a function of radiative current density for the two structures considered, and the gain saturates at a similar level in the N-based and equivalent conventional N-free QW structures considered [Fig. 4(b)]. The increased conduction band nonparabolicity also has little influence on the temperature dependence of the transparency carrier density for the dilute nitride structure considered, compared to the equivalent N-free structure.

We see from Fig. 4(a) that the differential gain decreases due to the incorporation of N. Small signal analysis of coupled carrier and photon density rate equations shows that the resonance frequency ω_r in a semiconductor laser is proportional to the square root of the differential gain: $\omega_r \propto \sqrt{dg/dn}$, where dg/dn is the differential gain with respect to the carrier density. We investigate in Fig. 5 how the differential gain varies with N content. The addition of either In or N reduces the energy gap E_g: In_yGa_{1-y}As behaves as a conventional III-V alloy, while the addition of N reduces the gap due to a repulsive anticrossing interaction between N resonant states and the conduction band edge [2], [3]. Because In atoms are larger than Ga atoms, an In_yGa_{1-y}As QW is compressively strained. By contrast, Ga-N bonds are about 20% shorter than Ga-As ones, so that the built-in compressive strain decreases rapidly with increasing N content. To find the optimal balance, we simultaneously changed the indium (In) and nitrogen (N) concentration, y and x, in a series of ideal 7-nm-wide QWs. In order to maintain the QW ground state transition energy e1-hh1 constant at 0.954 eV, in the range of nitrogen composition from $x = 0\%$ to $x = 3\%$, we have calculated a decrease in In composition from 55% to 30% [29]. We find that for a fixed broadening factor the calculated differential gain decreases with increasing N content, x, with the most rapid decrease observed at low x. As expected, the differential gain also decreases with increasing broadening

Authorized licensed use limited to: University of Surrey. Downloaded on May 26, 2009 at 10:31 from IEEE Xplore. Restrictions apply.

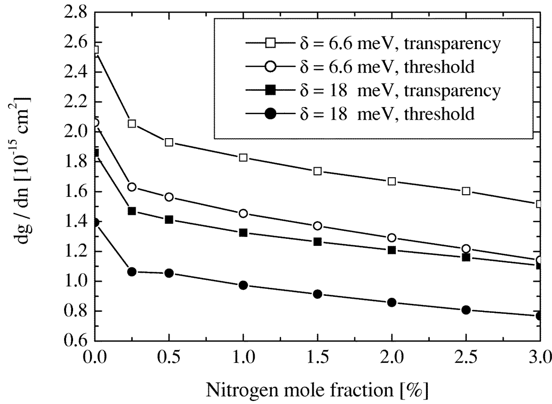

Fig. 5. Calculated variation of differential gain with N content: at transparency and with a broadening energy $\delta = 6.6$ meV (open squares); at threshold with $\delta = 6.6$ meV (open circles); at transparency with $\delta = 18$ meV (solid squares); and at threshold with $\delta = 18$ meV (solid circles).

factor. Because the measured broadening in InGaAsN increases with x [18], we conclude that the calculated threshold dg/dn value of $\sim 0.86 \times 10^{-15}$ cm^{-1} for $x = 0.02$ is only about 40% of the value which could be achieved in an ideal InGaAs 1.3-μm QW laser. The initial rapid reduction in differential gain (already notable at the first data point, $x = 0.25\%$) reflects the strong coupling between the N resonant band and the conduction band edge states, even at low x values. The matrix element (and differential gain) continue to decrease (but less rapidly) as we increase x from 0.5% to 3%, over which range the calculated compressive strain value also decreases from $\epsilon_{xx} \approx 3.2\%$ to 1.5%. To highlight influence of N, we note that over the same range of indium composition (from $\mathrm{In} = 50\%$ to $\mathrm{In} = 30\%$) Corzine *et al.* [30] reported a less rapid decreasing in differential gain (from 2.4×10^{-15} cm^2 to 1.8×10^{-15} cm^2) in N-free InGaAs QW lasers at transparency.

The carrier concentration at threshold (n_{th}) increases with increasing x, primarily due to the increase in the CB effective mass and reduction in the interband transition-matrix element when N is added. By contrast, the variation of J_{rad} is much weaker, being almost independent of N content [29]. Fig. 5 suggest that the optimal InGaAsN/GaAs QW laser device should contain minimal nitrogen, ideally being nitrogen-free! This is not possible because of the excessively large strain required to achieve 1.3-μm emission in a 7-nm InGaAs QW. We calculated the critical thickness h_c of an InGaAsN/GaAs QW as a function of in-plane strain, ϵ_{xx}, using the criteria in [31], estimating that we need $x > 1.5\%$ and $y < 39\%$ to achieve 1.3-μm emission in a pseudomorphic 7-nm-wide $\mathrm{In}_y\mathrm{Ga}_{1-y}\mathrm{As}_{1-x}\mathrm{N}_x$/GaAs QW structure. The N content can be further reduced by using narrower QWs, and also by growing tensile-strained layers above and below the QW, as demonstrated by Tansu *et al.* who achieved 1.3-μm emission with $x = 0.5\%$, a quantum well width of 6 nm, and utilizing strain-compensating $\mathrm{GaAs}_{0.85}\mathrm{P}_{0.15}$ tensile layers in the barrier region [32], [33].

D. Temperature Characteristics of Real InGaAsN QW Lasers

We turn in this section to analyze the characteristics of actual InGaAsN laser structures, using the theoretical models and insights established in the previous sections. We consider two different laser structures [34]: first, a 6.4-nm-wide single quantum well (SQW) laser with In and N-content of about 36% and 1.7%, respectively, and GaAs barriers; and secondly, a three quantum well (TQW) laser structure with well width 6.2 nm, $y(In) = 36\%$ and $x(N) = 1.8\%$, separated by 25 nm $\mathrm{In}_{0.045}\mathrm{Ga}_{0.955}\mathrm{As}_{0.985}\mathrm{N}_{0.015}$ barriers grown lattice-matched to GaAs. The SQW samples were fabricated into 50 μm-wide broad area devices and the TQW samples into 4-μm ridge waveguide devices. The emission wavelength at RT for the SQW and TQW lasers was found to be 1270 and 1290 nm, respectively.

The threshold material gain for the two structures was determined using (8). We took the experimentally determined internal loss values $\alpha_i \approx 4$ cm^{-1} and $\alpha_i \approx 10$ cm^{-1}, respectively [35]; we calculated the optical confinement factor to be $\Gamma_{\mathrm{TE}} = 1.5\%$ (SQW) and $= 5.3\%$ (TQW), with cavity lengths of $L = 750$ μm and $L = 700$ μm for the SQW and TQW case respectively, giving a threshold material gain of $g_{\mathrm{th}}^{\mathrm{SQW}} = 1280$ cm^{-1} and $g_{\mathrm{th}}^{\mathrm{TQW}} = 1000$ cm^{-1}. We assume in our analysis temperature-independent internal losses.

In our experimental setup the spontaneous emission (SE) spectrum was collected via a window milled into the n-contact (substrate) of the laser, using a silica-based 100-μm-diameter core multimode optical fiber and an optical spectrum analyzer (OSA). In this configuration, the integrated SE will not have undergone any significant amplification or absorption, and hence the collected pure SE will be directly proportional to the radiative current. By measuring the spontaneous recombination from a window in the substrate, we detect the spontaneous recombination of electrons with holes having $|x\rangle$- or $|y\rangle$- like (TE) character, assuming negligible photon scattering. Radiative recombination via $|z\rangle$-like (TM) valence band states will not be detected because the polarization vector is in the direction of light collection. The resulting integrated SE rate would, therefore, underestimate the total radiative current. However, due to the large heavy-hole $(1/2|x\rangle, 1/2|y\rangle)$ to light-hole $(1/6|x\rangle, 1/6|y\rangle, 2/3|z\rangle)$ subband splitting (114 meV) in these compressively-strained devices, the hole density in the light-hole band is expected to be negligible $(n_{\mathrm{hh1}}/n_{\mathrm{lh1}} \approx 40)$. Also the calculated ratio between the dipole matrix elements squared of these two VB states with the first electron states in the CB at $k_{\|} = 0$ is $|M_{\mathrm{e1-lh1}}|^2/|M_{\mathrm{e1-hh1}}|^2 = 0.66$. From our SE analysis we calculate that recombination via light-hole states resulting in SE of TM-like character is negligible compared to the TE-like SE occurring via the heavy-hole states. Hence, carrier recombination occurs via the heavy-hole band and is consequently of only $|x\rangle$- and $|y\rangle$-like character. We can, therefore, be confident that the measured SE spectra are representative of the total spontaneous recombination in the device.

To calculate accurately the dependence of the gain spectra on carrier concentration and on temperature, we first compared the experimentally measured SE spectra with those calculated using the 10-band $\mathbf{k}\cdot\mathbf{p}$ theory, including a sech line shape broadening function, (7), as shown in Fig. 6. The best fit to the spectra was got by changing the temperature dependent broadening parameter δ from 6.6 meV to 17 meV in the temperature range from 30

Authorized licensed use limited to: University of Surrey. Downloaded on May 26, 2009 at 10:31 from IEEE Xplore. Restrictions apply.

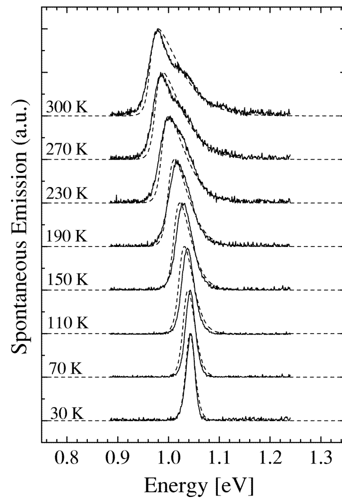

Fig. 6. Spontaneous emission spectra as a function of temperature. The dashed lines present calculated SE spectra.

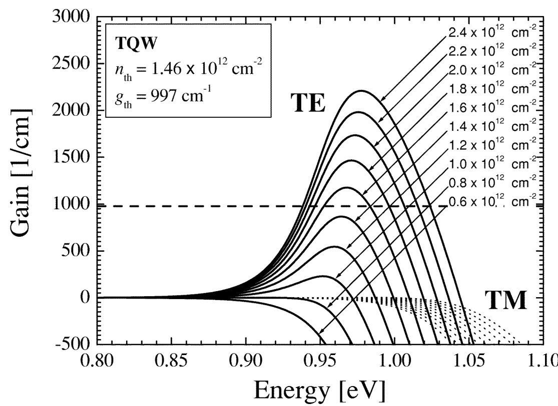

Fig. 7. Gain per QW spectra in the vicinity of the threshold for TQW structure: TE polarization—solid line and TM polarization—dashed line.

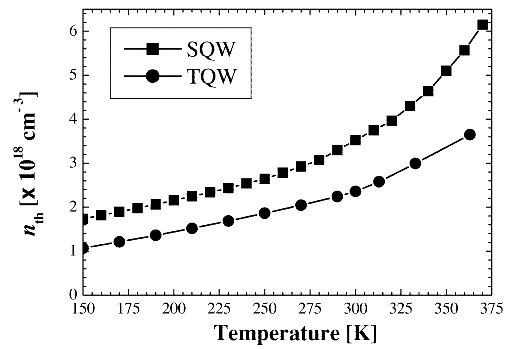

Fig. 8. Calculated carrier density at threshold for SQW (squares) and TQW (dots) devices.

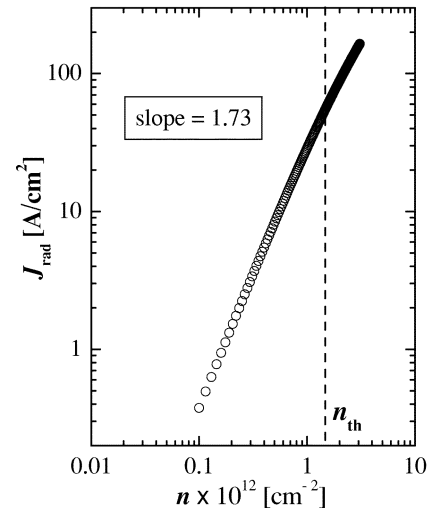

Fig. 9. Radiative current versus carrier concentration.

K to 300 K. The variation of the radiative current density $(J_{\rm rad})$ at threshold with temperature was then found by integrating over the SE spectrum at each value of T. Fig. 7 shows how the calculated material gain per QW varies as a function of carrier density in the TQW structure at 300 K. Our gain spectra agree well with those obtained using a full many-body theory, in which the many-body spectra were convolved with a Gaussian line function to model the (inhomogeneous) broadening observed by Hakki–Paoli measurements in InGaAsN devices [36]–[38].

We used data such as that in Fig. 7 to calculate the threshold carrier concentration, $n_{\rm th}$, as a function of temperature for the two structures considered. The calculated variation of $n_{\rm th}$, presented in Fig. 8, is higher for the SQW device, and increases more strongly at high temperature then in the TQW device, due to the lower optical confinement factor and consequently higher threshold material gain value.

To quantify the magnitudes of the monomolecular, radiative, and Auger recombination current paths throughout the structure we assume that the current injected into a laser operating at 1.3 μm may be written as:

$$J = qV(An + Bn^2 + Cn^3) \qquad (12)$$

where q is the electronic charge, V is the active region volume, A is the monomolecular recombination coefficient which describes recombination through traps and defects, B is the radiative or bimolecular recombination coefficient associated with spontaneous emission, and C is the Auger recombination coefficient. Radiative recombination involves the recombination of an electron in the conduction band with a hole in the valence band, resulting in the production of a photon. It is, thus, a two-carrier process and proportional to n^2 (for $n = p$) if Boltzmann statistics apply. In order to determine how well this relationship holds at the high injection levels observed in these devices we have plotted in Fig. 9, $J_{\rm rad}$ against carrier density n on log scales for the TQW laser. We evaluated that near threshold $J_{\rm rad} \propto n^{1.73}$, slightly lower than in 1.3-μm InGaAsP lasers where the gradient is 1.87 [39]. In Fig. 10(a) we plot the experimentally determined monomolecular current density (squares), the radiative current density (circles) and the Auger current density (triangles) as a function of temperature for the SQW structure [34], [40]. Additionally we plot in Fig. 10(a) the theoretically determined results (lines) where the temperature variation of $J_{\rm mono}$ was determined according to the model described in [34] and [41]. The theoretical temperature dependence of the Auger current is based upon the ten-band $\mathbf{k}\cdot\mathbf{p}$ theory discussed earlier, and is analogous to a model previously used for other material systems [42]–[44]. Using the experimental values for the current contributions at threshold from Fig. 10(a) and the theoretically deter-

Authorized licensed use limited to: University of Surrey. Downloaded on May 26, 2009 at 10:31 from IEEE Xplore. Restrictions apply.

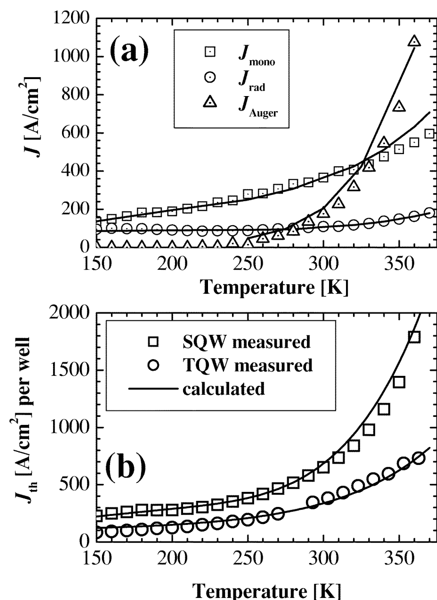

Fig. 10. (a) Monomolecular $J_{\rm mono}$, radiative $J_{\rm rad}$, and Auger $J_{\rm Auger}$ current versus temperature of SQW. (b) Measured total current per well versus temperature for SQW (open squares) and TQW (open circles), solid lines present calculated total current at threshold.

mined threshold carrier density from Fig. 8 we calculated the recombination coefficients A (monomolecular), B (radiative) and C (Auger) for the SQW device [34]. We derived at room temperature that $A = 11 \times 10^8$ s^{-1}, $B = 1 \times 10^{-10}$ cm^3 s^{-1} and $C = 4 \times 10^{-29}$ cm^6 s^{-1}. It should be noted that the values determined for the Auger coefficient are of similar magnitude to reported values of the Auger coefficient for 1.3-μm InGaAsP-based devices, for which C is typically in the range $1-8\times10^{-29}$ cm$^6 \cdot$ s^{-1} [45], [46]. This indicates that Auger recombination is also an important intrinsic recombination mechanism in InGaAsN. In Fig. 10(b) we plot the total current density per well at threshold for the SQW device (open squares) and a TQW device (open circles). It can be clearly observed that the threshold current in the SQW laser increases much faster with temperature than in the TQW device. Note that here we have neglected the effect of current spreading around the narrow (4 μm) ridge in the TQW devices. Whilst accurate determination of the degree of current spreading is complex, we can qualitatively understand how it would affect our results. By neglecting current spreading we effectively overestimate the threshold current density for the TQW ridge devices. This would make the difference between the TQW (ridge) and SQW (broad area) devices in Fig. 10 larger and hence would not affect our conclusions. Assuming that the recombination coefficients determined are the same in the SQW and the TQW device we can now use the calculated threshold carrier density, $n_{\rm th}$, of the TQW laser (from Fig. 8) to plot in Fig. 10(b) the expected variation of $J_{\rm th}$ with temperature for the TQW laser (open circles). We observe very good agreement, indicating that the different threshold carrier density of the SQW and the TQW devices can reasonably explain the different temperature variation of the threshold current.

We estimated the contribution of three current paths to the total threshold current and find that in this material, defect-related recombination is a significant current path over a wide temperature range, accounting for 55% of the total at room temperature (RT). We have also determined the absolute values of all three current paths over the entire temperature range considered, and further estimate that at RT the radiative and Auger recombination currents account for 20% and 25% of the total, respectively. Our measured temperature variations of $J_{\rm mono}$, $J_{\rm rad}$ and $J_{\rm Auger}$ are in good agreement with theoretical calculations based upon a 10-band $\mathbf{k}\cdot\mathbf{p}$ Hamiltonian. These results indicate that by removing the defect-related current path, the threshold current density could be approximately halved to values comparable with traditional InGaAsP/InP-based lasers making this material very attractive for VCSELs and other integrated GaAs-based devices.

IV. Conclusion

We have presented a theoretical analysis of ideal and real 1.3-μm InGaAsN lasers. Our analysis shows that a 10-band $\mathbf{k}\cdot\mathbf{p}$ Hamiltonian can successfully describe the band structure in dilute N-III-V structures. We predict that the addition of N reduces the peak gain and differential gain at fixed carrier density in an ideal dilute nitride QW structure when compared to an equivalent conventional structure. However, the gain saturation value and the peak gain as a function of radiative current density are largely unchanged due to the incorporation of N. Our calculations show that in order to maximize the differential gain and minimize the carrier concentration at threshold it is best to minimize the N composition, x in the QW, subject to critical thickness constraints.

From spontaneous emission measurements on real devices, we determine the absolute values of the radiative and nonradiative current components over the entire temperature range considered, and estimate that at room temperature the monomolecular, radiative and Auger recombination currents account respectively for 55%, 20%, and 25% of the total threshold current. These results indicate a large defect-related current contribution associated with the incorporation of nitrogen. In addition to nitrogen-related growth defects, possible causes of this loss could be the formation of various nitrogen next-neighbor configurations [47] or the incorporation of $\rm As_{Ga}$ antisite defects [48], [49] due to the low growth temperature required for the InGaAsN alloy.

Comparing our theoretical results on InGaAsN/GaAs with previous theoretical analysis of 1.3-μm InGaAsP/InP strained laser structures [50], we find that the InGaAsN material has a higher differential gain for the same amount of compressive strain ($\sim$1.5%: 0.8×10^{-15} cm^2 versus. 0.6×10^{-15} cm^2); optical gain ($\sim$1300 cm^{-1}: 0.8×10^{-15} cm^2 versus. 0.5×10^{-15} cm^2); and QW thickness (7 nm: 0.8×10^{-15} cm^2 versus. 0.6×10^{-15} cm^2), despite the significantly larger line broadening of 18 meV assumed in InGaAsN, compared to 6.6 meV in InGaAsP. For another strong competitor at 1.3-μm laser emission, InGaAlAs/InP strained lasers, at room temperature theoretical predictions suggest $dg/dn = 0.66 \times 10^{-15}$ cm^2 [51] while experimental measurements give a value of $dg/dn = 0.59 \times 10^{-15}$ cm^2 [52], for 1.46% compressively strained 5-nm wells in a MQW structure, but at a significantly

Authorized licensed use limited to: University of Surrey. Downloaded on May 26, 2009 at 10:31 from IEEE Xplore. Restrictions apply.

lower level of threshold gain ($\sim$460 cm^{-1}) than in InGaAsN lasers. At a comparable level of optical gain of $\sim$1000 cm^{-1} and at room temperature, the differential gain in InGaAlAs further drops to $dg/dn = 0.43 \times 10^{-15}$ cm^2 [51]. For a slightly different InGaAlAs structure, based on estimation from the relaxation oscillation frequency, Ishikawa *et al.* reported a value of $dg/dn = 1.1 \times 10^{-15}$ cm^2 at room temperature [53] which is above the values for InGaAsP and InGaAsN lasers.

The use of an InGaAsN alloy can allow greater compressive strain (up to 2.4%) compared to a typical InGaAsP/InP structure (where $\varepsilon_{xx} = 0.8\%$–1.1% for 1.3-μm emission and where at least 4 QWs are needed for successful operation) or compared to a typical InGaAlAs/InP structure (where ε_{xx} is up to $\sim$1.5% for 1.3-μm emission and where also MQW structures are needed for successful operation). Finally, InGaAsN also allows a deeper conduction band QW with stronger electron confinement, of benefit for higher temperature operation.

Appendix A

For completeness, Bloch basis functions of 10 band $\mathbf{k} \cdot \mathbf{p}$ Hamiltonian are provided as follows:

$$
\begin{aligned}
|u_1\rangle &= \left|\frac{1}{2}, +\frac{1}{2}\right\rangle = |s_N; \uparrow\rangle \\
|u_2\rangle &= \left|\frac{1}{2}, +\frac{1}{2}\right\rangle = |s; \uparrow\rangle \\
|u_3\rangle &= \left|\frac{3}{2}, +\frac{3}{2}\right\rangle = \frac{i}{\sqrt{2}}[|x; \uparrow\rangle + i|y; \uparrow\rangle] \\
|u_4\rangle &= \left|\frac{3}{2}, +\frac{1}{2}\right\rangle = \frac{i}{\sqrt{6}}[|x; \downarrow\rangle + i|y; \downarrow\rangle - 2|z; \uparrow\rangle] \\
|u_5\rangle &= \left|\frac{1}{2}, +\frac{1}{2}\right\rangle = \frac{i}{\sqrt{3}}[|x; \downarrow\rangle + i|y; \downarrow\rangle + |z; \uparrow\rangle] \\
|u_6\rangle &= \left|\frac{1}{2}, -\frac{1}{2}\right\rangle = -|s_N; \downarrow\rangle \\
|u_7\rangle &= \left|\frac{1}{2}, -\frac{1}{2}\right\rangle = -|s; \downarrow\rangle \\
|u_8\rangle &= \left|\frac{3}{2}, -\frac{3}{2}\right\rangle = -\frac{i}{\sqrt{2}}[|x; \downarrow\rangle - i|y; \downarrow\rangle] \\
|u_9\rangle &= \left|\frac{3}{2}, -\frac{1}{2}\right\rangle = +\frac{i}{\sqrt{6}}[|x; \uparrow\rangle - i|y; \uparrow\rangle + 2|z; \downarrow\rangle] \\
|u_{10}\rangle &= \left|\frac{1}{2}, -\frac{1}{2}\right\rangle = +\frac{i}{\sqrt{3}}[|x; \uparrow\rangle - i|y; \uparrow\rangle - |z; \downarrow\rangle].
\end{aligned}
$$

The set of states ($|u_1\rangle - |u_5\rangle$) transforms to the set of states ($|u_6\rangle - |u_{10}\rangle$), under the application of time-reversal operator for zinc-blende semiconductors, $\hat{T} = -i\sigma_y \hat{C} \hat{J}$, where σ_y is the spin Pauli matrix which flips the spin component, $\hat{C}$ is the complex conjugation operator, and $\hat{J}$ is the inversion about midpoint between nearest neighbors ($s \mapsto -s, p \mapsto p$). Due to this operator the system now posses Kramers symmetry.

Acknowledgment

The authors would like to thank M. Kamal-Saadi, P. Klar, and A. Lindsay for useful discussions.

References

[1] M. Kondow, T. Kitatani, S. Nakatsuka, M. C. Larson, K. Nakahara, Y. Yazawa, M. Okai, and K. Uomi, "GaInNAs: A novel material for long-wavelength semiconductor lasers," *IEEE J. Select. Topic Quantum Electron.*, vol. 3, pp. 719–730, June 1997.

[2] W. Shan, W. Walukiewicz, J. W. Ager, E. E. Haller, J. F. Geisz, D. J. Friedman, J. M. Olson, and S. R. Kurtz, "Band anticrossing in GaInNA's alloys," *Phys. Rev. Lett.*, vol. 82, pp. 1221–1224, 1999.

[3] B. N. Murdin, A. R. Adams, P. Murzyn, C. R. Pidgeon, I. V. Bradley, J.-P. R. Wells, Y. H. Matsuda, N. Miura, T. Burke, and A. D. Johnson, "Band anticrossing in dilute InNSb," *Appl. Phys. Lett.*, vol. 81, pp. 256–258, 2002.

[4] K. D. Choquette *et al.*, "Room temperature continuous wave InGaAsN quantum well vertical-cavity lasers emitting at 1.3 μm," *Electron. Lett.*, vol. 36, pp. 1388–1390, 2000.

[5] G. Steinle, H. Riechert, and A. Y. Egorov, "Monolithic VCSEL with InGaAsN active region emitting at 1.28 μm and CW output power exceeding 500 μW at room temperature," *Electron. Lett.*, pp. 93–95, 2001.

[6] T. Kageyama *et al.*, "Room temperature continuous-wave operation of GaInNAs/GaAs VCSELs grown by chemical beam epitaxy with output power exceeding 1 mW," *Electron. Lett.*, vol. 37, pp. 225–226, 2001.

[7] E. O. Kane, "The $\mathbf{k} \cdot \mathbf{p}$ method," *Semiconduct. Semimetal.*, vol. 1, pp. 75–100, 1966.

[8] A. T. Meney, B. Gonul, and E. P. O'Reilly, "Evaluation of different approximations used in envelope-function method," *Phys. Rev. B*, vol. 50, pp. 10 893–10 904, 1994.

[9] E. P. O'Reilly, A. Lindsay, S. Tomić, and M. Kamal-Saadi, "Tight-binding and $\mathbf{k} \cdot \mathbf{p}$ models for the electronic structure of Ga(In)NA's and related alloys," *Semicond. Sci. Technol.*, vol. 17, pp. 870–879, 2002.

[10] A. Lindsay and E. P. O'Reilly, "Theory of the electronic structure of GaInNAs," in *Proc. 25th ICPS*, vol. 87, N. Miura and T. Ando, Eds., 2001, p. 63.

[11] D. Ahn and S. L. Chuang, "Optical gain and gain suppression of quantum-well lasers with valence band mixing," *IEEE J. Quantum Electron.*, vol. 26, pp. 13–24, Jan. 1990.

[12] S. L. Chuang, *Physics of Optolectronic Devices*. New York: Wiley, 1995.

[13] W. W. Chow and S. W. Koch, *Semiconductor—Laser Fundamentals*. Berlin, Germany: Springer-Verlag, 1999.

[14] M. Silver and E. P. O'Reilly, "Optimization of Long Wavelength InGaAsP Strained Quantum-Well Lasers," *IEEE J. Quantum Electron.*, vol. 31, pp. 1193–1200, July 1995.

[15] S. Sakai, Y. Ueta, and Y. Terauchi, "Band-gap energy and band lineup of III–V-alloy semiconductors incorporating nitrogen and boron," *Jpn. J. Appl. Phys.*, pt. 1, vol. 32, p. 4413, 1993.

[16] L. Bellaiche, S.-H. Wei, and A. Zunger, "Composition dependence of interband transition intensities in GaPN, GaAsN, and GaPAs alloys," *Phys. Rev. B*, vol. 56, pp. 10 233–10 240, 1997.

[17] I. A. Buyanova, G. Pozina, P. N. Hai, W. M. Chen, H. P. Xin, and C. W. Tu, "Type I band alignment in the GaN_xAs_{1-x}/GaAs quantum wells," *Phys. Rev. B*, vol. 63, 2000.

[18] P. J. Klar, H. Grüning, W. Heimbrodt, G. Weiser, J. Koch, K. Volz, W. Stolz, S. W. Koch, S. Tomić, S. A. Choulis, T. J. C. Hosea, E. P. O'Reilly, M. Hofmann, J. Hader, and J. V. Moloney, "Interband transitions of quantum wells and device structures containing Ga(N, As) and (Ga,In)(N, As)," *Semicond. Sci. Technol.*, vol. 17, pp. 830–842, 2002.

[19] C. G. Van de Walle, "Band lineups and deformation potentials in the model-solid theory," *Phys. Rev. B*, vol. 39, pp. 1871–1883, 1989.

[20] P. J. Klar, H. Grüning, W. Heimbrodt, J. Koch, W. Stolz, P. M. A. Vicente, A. M. Kamal Saadi, A. Lindsay, and E. P. O'Reilly, "Pressure and temperature dependent studies of GaN_xAs_{1-x}/GaAs quantum well structures," *Phys. Stat. Sol. B*, vol. 223, pp. 163–169, 2001.

[21] S. A. Choulis, S. Tomić, E. P. O'Reilly, and T. J. C. Hosea, "Determining the band-structure of an InGaNAs/GaAs semiconductor laser structure using nondestructive photomodulated reflectance measurements and $\mathbf{k} \cdot \mathbf{p}$ studies," *Solid. State Commun.*, vol. 125, pp. 155–159, 2003.

[22] S. A. Choulis, T. J. C. Hosea, S. Tomić, M. Kamal-Saadi, A. R. Adams, E. P. O'Reilly, B. A. Weinstein, and P. J. Klar, "Electronic structure of $In_yGa_{1-y}As_{1-x}N_x$/GaAs multiple quantum wells in the dilute-N regime from pressure and $\mathbf{k} \cdot \mathbf{p}$ studies," *Phys. Rev. B*, vol. 66, 2002.

[23] P. J. Klar, H. Grüning, J. Koch, S. Schäfer, K. Volz, W. Stolz, W. Heimbrodt, A. M. Kamal Saadi, A. Lindsay, and E. P. O'Reilly, "(Ga, In)(N, As)-fine structure of the band gap due to nearest-neighbor configurations of the isovalent nitrogen," *Phys. Rev. B*, vol. 64, 2001.

[24] A. Polimeni, M. Capazzi, M. Geddo, M. Fischer, M. Reinhardt, and A. Forchel, "Effect of nitrogen on the temperature dependence of the energy gap in InGaAsN/GaAs single quantum wells," *Phys. Rev. B*, vol. 63, 2001.

Authorized licensed use limited to: University of Surrey. Downloaded on May 26, 2009 at 10:31 from IEEE Xplore. Restrictions apply.

[25] P. Perlin, P. Wisniewski, C. Skierbiszewski, T. Suski, E. Kaminska, S. G. Subramanya, E. R. Weber, D. E. Mars, and W. Walukiewicz, "Interband optical absorption in free standing layer of $Ga_{0.96}In_{0.04}As_{0.99}N_{0.01}$," *Appl. Phys. Lett.*, vol. 76, pp. 1279–1281, 2000.
[26] I. Suemune, K. Uesugi, and W. Walukiewicz, "Role of nitrogen in the reduced temperature dependence of band-gap energy in GaNAs," *Appl. Phys. Lett.*, vol. 77, pp. 3021–3023, 2000.
[27] S. Tomić and E. P. O'Reilly, "Gain characteristics of ideal dilute nitride quantum well lasers," *Physica E*, vol. 13, pp. 1102–1105, 2002.
[28] W. W. Chow, E. D. Jones, N. A. Modine, A. A. Allerman, and S. R. Kurtz, "Laser gain and threshold properties in compressive-strained and lattice-matched GaInNAs/GaAs quantum wells," *Appl. Phys. Lett.*, vol. 75, pp. 2891–2893, 1999.
[29] S. Tomić and E. P. O'Reilly, "Optimization of material parameters in 1.3 μm InGaAsN/GaAs lasers," *IEEE Photon. Technol. Lett.*, vol. 15, pp. 6–8, Jan. 2003.
[30] S. W. Corzine, R. H. Yan, and L. A. Coldren, "Theoretical gain in strained InGaAs/AlGaAs quantum wells including valence-band mixing effect," *Appl. Phys. Lett.*, vol. 57, pp. 2835–2837, 1990.
[31] E. P. O'Reilly, "Valence band engineering in strained-layer structures," *Semicond. Sci. Technol.*, vol. 4, pp. 121–137, 1989.
[32] N. Tansu, N. J. Kirsch, and L. J. Mawst, "Low-threshold-current-density 1300-nm dilute-nitride quantum well lasers," *Appl. Phys. Lett.*, vol. 81, pp. 2523–2525, 2002.
[33] N. Tansu and L. J. Mawst, "Temperature sensitivity of 1300-nm InGaAsN quantum-well lasers," *IEEE Photon. Technol. Lett.*, vol. 14, pp. 1052–1054, Aug. 2002.
[34] R. Fehse, S. Tomić, A. R. Adams, S. J. Sweeney, E. P. O'Reilly, A. Andreev, and H. Riechert, "A quantitative study of radiative, Auger, and defect related recombination processes in 1.3- μm GaInNAs-based quantum-well lasers," *IEEE J. Select. Topic Quantum Electron.*, vol. 8, pp. 801–810, July/Aug. 2002.
[35] H. Riechert, A. Y. Egorov, D. Livshits, B. Borchert, and S. Illek, "InGaAsN/GaAs heterostructures for long-wavelength light-emitting devices," *Nanotechnol.*, vol. 11, pp. 201–205, 2000.
[36] M. Hofmann *et al.*, "Gain spectra of (GaIn)(NAs) laser diodes for the 1.3-μm-wavelength regime," *Appl. Phys. Lett.*, vol. 78, pp. 3009–3011, 2001.
[37] M. R. Hofmann *et al.*, "Emission dynamics and optical gain of 1.3- μm (GaIn)(NAs)/GaAs lasers," *IEEE J. Quantum. Electron.*, vol. 38, pp. 213–221, Feb. 2002.
[38] J. Hadera, S. W. Koch, J. V. Moloney, and E. P. O'Reilly, "Gain in 1.3 μm materials: InGaNAs and InGaPAs semiconductor quantum-well lasers," *Appl. Phys. Lett.*, vol. 77, pp. 630–632, 2000.
[39] A. F. Phillips, S. J. Sweeney, A. R. Adams, and P. J. A. Thijs, "The temperature dependence of 1.3- and 1.5-μm compressively strained InGaAs(P) MQW semiconductor lasers," *IEEE J. Select. Topic Quantum Electron.*, vol. 5, pp. 401–412, May/June 1999.
[40] R. Fehse, A. R. Adams, S. J. Sweeney, S. Tomić, H. Riechert, and A. Ramakrishnan, "Carrier recombination processes in MOVPE and MBE grown 1.3 μm GaInNAs edge emitting lasers," *Solid State Electron.*, vol. 47, pp. 501–506, 2003.
[41] R. Fehse, S. Jin, S. J. Sweeney, A. R. Adams, E. P. O'Reilly, A. Y. Egorov, H. Riechert, and S. Illek, "Evidence for a large monomolecular recombination contribution to the threshold current in 1.3 μm GaInNAs semiconductor lasers," *Electron. Lett.*, vol. 37, pp. 1518–1519, 2001.
[42] A. D. Andreev and G. G. Zegrya, "Theoretical study of thresholdless Auger recombination in compressively strained InAlAsSb/GaSb quantum wells," *Appl. Phys. Lett.*, vol. 70, pp. 601–603, 1997.
[43] A. D. Andreev and D. V. Donetsky, "Analysis of temperature dependence of the threshold current in 2.3–2.6 μm InGaAsSb/AlGaAsSb quantum-well lasers," *Appl. Phys. Lett.*, vol. 74, pp. 2743–2745, 1999.
[44] A. D. Andreev, E. P. O'Reilly, A. R. Adams, and T. Ashley, "Theoretical performance and structure optimization of 3.5–4.5 μm InGaSb/InGaAlSb multiple quantum well lasers," *Appl. Phys. Lett.*, vol. 78, pp. 2640–2642, 2001.
[45] G. P. Agrawal and N. K. Dutta, *Long Wavelength Semiconductor Lasers*. New York: Van Nostrand Reinhold, 1986.
[46] J. M. Pikal, C. S. Menoni, H. Temkin, P. Thiagarajan, and G. Y. Robinson, "Carrier lifetime and recombination in long-wavelength quantum-well lasers," *IEEE J. Select. Topics Quantum. Electron.*, vol. 5, pp. 613–619, May/June 1999.
[47] P. R. C. Kent and A. Zunger, "Nitrogen pairs, triplets, and clusters in GaAs and GaP," *Appl. Phys. Lett.*, vol. 79, pp. 2339–2341, 2001.
[48] N. Q. Thinh, I. A. Buyanova, P. N. Hai, and W. M. Chen, "Signature of an intrinsic point defect in GaN_xAs_{1-x}," *Phys. Rev. B*, vol. 63, 2001.
[49] N. Q. Thinh, I. A. Buyanova, and W. M. Chen, "Formation of nonradiative defects in molecular beam epitaxial GaN_xAs_{1-x} studied by optically detected magnetic resonance," *Appl. Phys. Lett.*, vol. 79, pp. 3089–3091, 2001.
[50] S. Seki *et al.*, "Theoretical-analysis of pure effects of strain and quantum confinement on differential gain in InGaAsP/InP strained-layer quantum-well lasers," *IEEE J. Quantum Electron.*, vol. 30, pp. 500–510, Feb. 1994.
[51] J. W. Pan and J. I. Chyi, "Theoretical study of the temparature dependance of 1.3 μm AlGaInAs-InP multiple quantum well lasers," *IEEE J. Quantum Electron.*, vol. 32, pp. 2133–2138, Dec. 1996.
[52] C. E. Zah, M. C. Wang, R. Bhat, T. P. Lee, S. L. Chuang, Z. Wang, D. Darby, D. Flanders, and J. J. Hsieh, "High-temperature modulation dynamics of 1.3 μm AlGaInAs/InP compressive-strained multiple-quantum-well lasers," *Proc. 14th IEEE Int. Semiconductor Laser Conf.*, pp. 215–216, 1994.
[53] T. Ishikawa, T. Higashi, T. Uchida, T. Fujii, T. Yamamoto, H. Shoji, and M. Kobayashi, "Evaluation of differential gain of 1.3 μm AlGaInAs/InP strained MQW lasers," in *Proc. 10th Int. Conf. Indium Phosphide Related Materials*, Tsukuba, Japan, 1998, pp. 729–732.

Stanko Tomić was born in Belgrade, Yugoslavia, in 1967. He received the B.S.E.E., M.Sc., and the Ph.D. degrees in electrical engineering from University of Belgrade, in 1993, 1996, and 1998, respectively.

In 1993, he joined VINČA Institute of Nuclear Sciences, Belgrade. He has been engaged in research of intersubband optical nonlinearities in semiconductor quantum wells and optically pumped intersubband lasers. As a Research Fellow in the Optoelectronics Devices and Materials Group at the University of Surrey, Guildford, U.K., he was working on theory of (In,Ga)(As,N) materials and optoelectronic devices. Currently, he is with Department of Physics and Astronomy, University of Sheffield, Sheffield, U.K., working on theory of quantum cascade lasers. His research interests include physics of gain and loss mechanism in interband quantum well lasers, quantum cascade lasers, intersubband optical nonlinearities in semiconductor quantum structures, as well as band structure calculations of III–V materials with diluted nitrogen content.

Eoin P. O'Reilly (M'03) was born in Dublin, Ireland, in 1957. He received the B.A. (MOD) degree in physics from Trinity College, Dublin, Ireland, and the Ph.D. degree (in electronic properties of defects in amorphous semiconductors) from the University of Cambridge, Cambridge, U.K., in 1978 and 1982, respectively.

He joined the Department of Physics, University of Surrey, Guildford, U.K., as a Lecturer in 1984. He was promoted to Professor of Physics in 1995 and was Head of the Physics Department from 1997 to 2001. In September 2001, he joined the National Microelectronics Research Centre (NMRC), Cork, Ireland, as a Research Professor, where he now leads one of the first projects funded by Science Foundation Ireland, to investigate the physics of next-generation photonic devices.

Robin Fehse was born in Hannover, Germany, in 1971. He received the Diplom der Physik degree from the Philipps-Universität, Marburg, Germany, in 1999 and the Ph.D. degree in semiconductor laser physics from the University of Surrey, Guildford, U.K. in 2003, where he is currently working as a Postdoctoral Researcher.

His research interests are in the areas of optical and magneto-optical spectroscopy on III-V semiconductor materials and more recently investigating the properties of 1.3 μm GaInNAs-based semiconductor edge-emitting and vertical cavity surface emitting lasers and their dependence on temperature and hydrostatic pressure.

Dr. Fehse is a Member of the Institute of Physics (U.K.) and of the Deutsche Physikalische Gesellschaft (Germany).

Authorized licensed use limited to: University of Surrey. Downloaded on May 26, 2009 at 10:31 from IEEE Xplore. Restrictions apply.

Stephen John Sweeney (S'98–M'99) was born in Luton, U.K., in 1973. He received the B.Sc. (Hons.) degree in applied physics and the Certificate in Education from the University of Bath, Bath, U.K., in 1995 and the Ph.D. degree in semiconductor laser physics at the University of Surrey, Surrey, U.K., in 1999.

After two years as a Postdoctoral Researcher he worked as a Scientist for Marconi Optical Components on the development of signal and pump sources for telecommunications applications. He is currently a Lecturer in semiconductor laser physics at the University of Surrey. His research interests include understanding the gain and loss processes underpinning the performance of semiconductor lasers utilizing a combination of novel experimental techniques coupled with complementary theoretical modeling. His current research activities include long-wavelength InGaAs(P)-, AlGaInAs-, and GaInNAs-based MQW semiconductor lasers for cooler-free applications and future GaAs-based vertically integrated devices. He is also interested in failure mechanisms in high power semiconductor lasers for fiber amplifiers and has worked on both visible VCSEL and edge-emitting lasers as well as 1.3-µm quantum dot structures.

Dr. Sweeney is a Chartered Physicist and a member of The Institute of Physics, London, U.K.

Alfred R. Adams (M'82–SM'00–F'01) was born in the U.K., in 1939. He received the B. Sc., Ph.D., and D.Sc. degrees in physics from the University of Leicester, Leicester, U.K., in 1961, 1964, and 1986, respectively. After completing his Ph.D. research into the electrical and optical properties of orthorhombic sulphur he spent two years at the University of Karlsruhe, Karlsruhe, Germany, studying the thermal and thermoelectric properties of selenium and tellurium.

In 1967, he joined the University of Surrey, Surry, U.K., where he is now a Professor of physics and Leader of the Optoelectronic Devices and Materials research group. Semiconductor lasers have been one of his major interests since 1980 when he spent sabbatical leave at Tokyo Institute of Technology, Tokyo, Japan. He held the Hitachi Visiting Chair at Tokyo Institute of Technology in 1992 and was CNRS Visiting Researcher at the University of Montpellier in 1993.

Dr. Adams was awarded the Duddell Medal and Prize by the Institute of Physics, U.K., in 1995 for his work on strained-layer lasers. He is a Fellow of the Institute of Physics, London, U.K., and the Institute of Electrical Engineers, U.K. In 1996, he was Elected Fellow of the Royal Society.

Aleksey D. Andreev, photograph and biography not available at the time of publication.

Stelios A. Choulis was born in Athens, Greece, in 1974. He received the B.Sc. (Honc.) degree in physics from the University of Patras, Patras, Greece, in 1995. and the M.Sc. and Ph.D. degrees from the University of Surrey, Guildford, U.K., in 1996 and 2001, respectively.

Following a one-year Postdoctoral Rsearch Position of the University of Surrey, he joined the Department of Physics, Blackett Laboratory, Imperial College, London, U.K. His research interests are in the areas of organic and inorganic semiconductors with an emphasis on their optoelectronic applications.

Thomas J. C. Hosea received the Ph.D. degree from the University of Edinburgh, Edinburgh, U.K., in 1978.

At the University of Surrey, Guildford, U.K., where he is now Senior Lecturer in Optoelectronics (equivalent to Associate Professor), he has established a program of research into the spectroscopic investigation of the band structure of low-dimensional semiconductor devices and nanostructures with operating wavelengths in the range of 300–1500 nm, including nitrides and quantum dots, and has pioneered modulated reflectance as a nondestructive characterization tool for vertical-cavity surface-emitting lasers and resonant-cavity LEDs

Henning Riechert, photograph and biography not available at the time of publication.

Authorized licensed use limited to: University of Surrey. Downloaded on May 26, 2009 at 10:31 from IEEE Xplore. Restrictions apply.